KUKA KR500 Kinematics and Motion Planning

Max Heil
The Ohio State University Department of Mechanical & Aerospace Engineering

***Abstract*—This short paper focuses on finding the forward and inverse kinematics of the KUKA KR500 R2830 robot for theme park applications. I verify the kinematics through various methods and implement them into an interactive app.**

I. Introduction

Large-scale robotic theme park rides (typically called dark-rides) demand repeatable, high-dynamic motion under strict safety constraints. To study this in a controlled setting, this work models the system as a fixed-base serial manipulator and uses the KUKA KR500 R2830 as a proxy for KR500 "Robo-Coaster" variants with unavailable proprietary data. With a modified Denavit–Hartenberg parameterization, we derive forward kinematics and a closed-form inverse kinematics solution enabled by the robot's spherical wrist: the wrist center solves (q_1, q_2, q_3) and wrist orientation solves (q_4, q_5, q_6), yielding up to eight non-singular branches with joint-limit filtering and singularity handling. We then implement an interactive motion-planning app for two-waypoint motion using MoveJ (joint-space interpolation) and MoveL (linear Cartesian interpolation with log/exp orientation interpolation). The app outputs joint trajectories and real-time 3-D animation for rapid evaluation of branch selection, continuity, and path feasibility.

II. Robot Model and Notation

The system is modeled as a 6-DOF serial, revolute-joint industrial manipulator (KUKA KR500 R2830). A fixed inertial base frame $\{0\}$ is attached to the robot pedestal, and the tool frame $\{6\}$ is attached to the end-effector flange. Link frames $\{1\}, \ldots, \{6\}$ are assigned using the modified Denavit–Hartenberg (DHM) convention. The corresponding coordinate frame is shown in Fig 1.

Let the joint configuration be

$$\mathbf{q} \triangleq \begin{bmatrix} q_1 & q_2 & q_3 & q_4 & q_5 & q_6 \end{bmatrix}^\mathsf{T}, \tag{1}$$

where each q_i is a joint angle (rad). The forward kinematics map returns the pose of the tool frame relative to the base as the homogeneous transform ${}^0T_6(\mathbf{q}) \in SE(3)$, written in block form as

$${}^0T_6(\mathbf{q}) \triangleq \begin{bmatrix} R_{06}(\mathbf{q}) & p_{06}(\mathbf{q}) \\ \mathbf{0}^\mathsf{T} & 1 \end{bmatrix}, \tag{2}$$

where $R_{06} \in SO(3)$ is the rotation matrix and $p_{06} \in \mathbb{R}^3$ is the position vector of the tool-frame origin expressed in $\{0\}$. Unless otherwise stated, lengths are expressed in millimetres and angles in radians throughout the paper.

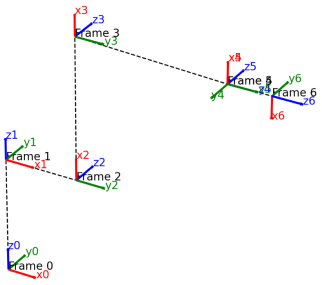

Fig. 1. KUKA KR500 R2830 Coordinate Frame from DHM.

III. Forward Kinematics

A. DH Parameters

The KR500 R2830 is parameterized using the DHM convention. For each joint i, the DHM parameter set is

$$[\alpha_i,\ a_i,\ d_i,\ \theta_{0,i}], \tag{3}$$

where α_i is the twist angle, a_i is the link length, d_i is the link offset, and $\theta_{0,i}$ is a constant joint-angle offset. The numerical values used in this work are listed in Table I.

TABLE I
KUKA KR500 R2830 Modified DH Table.

i	a_i [mm]	α_i [rad]	d_i [mm]	θ_i [rad]	Type
1	0	0	1045	0	R
2	500	$-\pi/2$	0	0	R
3	1300	0	0	$-\pi/2$	R
4	-55	$-\pi/2$	1025	0	R
5	0	$\pi/2$	0	0	R
6	0	$-\pi/2$	290	π	R

To match the reference model's joint sign convention, the effective joint angle used in the per-link transform is

$$\theta_i(\, q_i\,) = \theta_{0,i} + s_i\, q_i, \tag{4}$$

with sign vector

$$\mathbf{s} \triangleq \begin{bmatrix} s_1 & s_2 & s_3 & s_4 & s_5 & s_6 \end{bmatrix}^\mathsf{T} = \begin{bmatrix} -1 & 1 & 1 & -1 & 1 & -1 \end{bmatrix}^\mathsf{T}. \tag{5}$$

Equivalently, the six effective angles are

$$\theta_1 = -q_1, \quad \theta_2 = q_2, \quad \theta_3 = q_3 - \frac{\pi}{2}, \quad \theta_4 = -q_4, \quad \theta_5 = q_5, \quad \theta_6 = \pi - q_6. \tag{6}$$

B. Homogeneous Transformations

The forward kinematics are built from a sequence of homogeneous transforms between consecutive link frames. Using the modified DH convention, the transform from frame $(i-1)$ to frame i is defined as ${}^{i-1}T_i(\theta_i) \in SE(3)$ with

$$ {}^{i-1}T_i = \begin{bmatrix} c_i & -s_i & 0 & a_i \\ s_i c_{\alpha_i} & c_i c_{\alpha_i} & -s_{\alpha_i} & -s_{\alpha_i} d_i \\ s_i s_{\alpha_i} & c_i s_{\alpha_i} & c_{\alpha_i} & c_{\alpha_i} d_i \\ 0 & 0 & 0 & 1 \end{bmatrix}, \tag{7} $$

where $c_i = \cos(\theta_i)$, $s_i = \sin(\theta_i)$, $c_{\alpha_i} = \cos(\alpha_i)$, and $s_{\alpha_i} = \sin(\alpha_i)$. Substituting the KR500 DH parameters (Table I) and the effective angles in (4) yields the six link transforms ${}^0T_1, \ldots, {}^5T_6$. For example, the first two transforms simplify immediately because $\alpha_1 = 0$ and $\alpha_2 = -\pi/2$:

$$ {}^0T_1 = \begin{bmatrix} \cos(\theta_1) & -\sin(\theta_1) & 0 & 0 \\ \sin(\theta_1) & \cos(\theta_1) & 0 & 0 \\ 0 & 0 & 1 & 1045 \\ 0 & 0 & 0 & 1 \end{bmatrix}, \tag{8} $$

$$ {}^1T_2 = \begin{bmatrix} \cos(\theta_2) & -\sin(\theta_2) & 0 & 500 \\ 0 & 0 & 1 & 0 \\ -\sin(\theta_2) & -\cos(\theta_2) & 0 & 0 \\ 0 & 0 & 0 & 1 \end{bmatrix}. \tag{9} $$

The end-effector pose is obtained by chaining the six link transforms:

$$ {}^0T_6(\mathbf{q}) = {}^0T_1\, {}^1T_2\, {}^2T_3\, {}^3T_4\, {}^4T_5\, {}^5T_6. \tag{10} $$

To obtain a closed form, the product in (10) is expanded symbolically and simplified using trigonometric shorthand. Define $c1 = \cos q_1$, $s1 = \sin q_1$, $c4 = \cos q_4$, $s4 = \sin q_4$, $c5 = \cos q_5$, $s5 = \sin q_5$, $c_{23} = \cos(q_2 + q_3)$, and $s_{23} = \sin(q_2 + q_3)$, along with the scalar

$$ B \triangleq 500 + 1300 \cos q_2 + 1025\, c_{23} - 55\, s_{23}. \tag{11} $$

In the resulting closed form, the rotation matrix R_{06} is the upper-left 3×3 block of ${}^0T_6$. The third column of R_{06} (used directly in the position expression below) is

$$ \begin{aligned} R_{13} &= -s5\,(s1\, s4 + s_{23}\, c1\, c4) + c5\,(c1\, c_{23}), \\ R_{23} &= -s5\,(-s1\, s_{23}\, c4 + s4\, c1) + c5\,(-s1\, c_{23}), \\ R_{33} &= -s5\,(c4\, c_{23}) + c5\,(-s_{23}). \end{aligned} \tag{12} $$

Likewise, the position vector p_{06} is the upper-right 3×1 block of ${}^0T_6$. First, the origin of frame 4 in the base frame is

$$ p_{04} = \begin{bmatrix} c1\, B \\ -s1\, B \\ 1045 - 1300 \sin q_2 - 1025\, s_{23} - 55\, c_{23} \end{bmatrix}, \tag{13} $$

and since the final link has $a_6 = 0$ and $d_6 = 290$, the end-effector origin is

$$ p_{06} = p_{04} + 290 \begin{bmatrix} R_{13} & R_{23} & R_{33} \end{bmatrix}^{\mathsf{T}}. \tag{14} $$

Finally, the closed-form homogeneous transform is written compactly as

$$ {}^0T_6(q) = \begin{bmatrix} R_{06}(q) & p_{06}(q) \\ 0 & 1 \end{bmatrix}, \tag{15} $$

where $R_{06}(q)$ and $p_{06}(q)$ follow from the expanded product in (10) using the shorthand in (11)–(14).

For the complete in-depth derivation of the FK, please refer to the repository on Github: Click here for Github link.

C. FK Validation

The forward-kinematics (FK) implementation was validated by comparing the MATLAB-computed end-effector pose to a RoboDK reference model. For each test configuration $\mathbf{q}^{(k)}$ (entered in degrees in RoboDK and converted to radians internally in MATLAB), MATLAB computes ${}^0T_{6,\mathrm{MAT}}(\mathbf{q}^{(k)})$ using the DHM parameters and the FK chain in (10). The corresponding RoboDK pose ${}^0T_{6,\mathrm{RDK}}(\mathbf{q}^{(k)})$ was obtained by setting the same joint angles in RoboDK and copying the resulting 4×4 pose matrix. A larger suite of joint configurations was evaluated (including home, zero, mixed-angle, and additional stress tests); due to space constraints, only three representative cases are reported here.

Agreement was quantified using both translational and rotational residuals. Let $p_{\mathrm{MAT}}, R_{\mathrm{MAT}}$ and $p_{\mathrm{RDK}}, R_{\mathrm{RDK}}$ denote the position and rotation blocks extracted from the two transforms. The position error is

$$ e_p^{(k)} \triangleq \left\| p_{\mathrm{MAT}}^{(k)} - p_{\mathrm{RDK}}^{(k)} \right\|_2, \tag{16} $$

and the orientation error is computed from the principal angle of the relative rotation

$$ e_R^{(k)} \triangleq \cos^{-1}\left(\frac{\mathrm{tr}\left(\left(R_{\mathrm{MAT}}^{(k)} \right)^{\mathsf{T}} R_{\mathrm{RDK}}^{(k)} \right) - 1}{2} \right), \tag{17} $$

reported in degrees after conversion. The comparison between the two, using RoboDK as the ground-truth, was nearly indistinguishable, as seen in Table II.

TABLE II
FK VALIDATION SUMMARY FOR THREE REPRESENTATIVE CASES (MATLAB VS. ROBODK).

Case	$\mathbf{q}$ [deg]	e_p [mm]	e_R [deg]
1	[0, −90, 90, 0, 0, 0]	10^{-13}	10^{-6}
2	[30, −20, 40, 10, −30, 60]	10^{-13}	10^{-6}
3	[−120, 10, −80, −150, 90, −120]	10^{-13}	10^{-6}

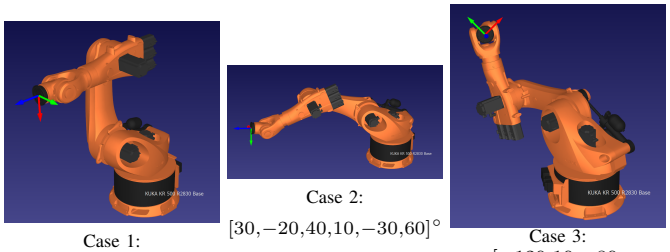

Case 1: [0,−90,90,0,0,0]°

Case 2: [30,−20,40,10,−30,60]°

Case 3: [−120,10,−80, −150,90,−120]°

Fig. 2. RoboDK visualizations for the three representative FK validation cases.

For completeness, the MATLAB and RoboDK homogeneous transforms for the three cases are shown below. In each case, ${}^0T_{6,\mathrm{MAT}}(\mathbf{q}^{(k)})$ matches ${}^0T_{6,\mathrm{RDK}}(\mathbf{q}^{(k)})$ to numerical precision.

$$
{}^{0}T_{6,\mathrm{MAT}}\Big(\mathbf{q}^{(1)}\Big) = {}^{0}T_{6,\mathrm{RDK}}\Big(\mathbf{q}^{(1)}\Big) =
\begin{bmatrix}
-0.000000 & -0.000000 & 1.000000 & 1815.000000 \\
-0.000000 & 1.000000 & 0.000000 & 0.000000 \\
-1.000000 & -0.000000 & -0.000000 & 2290.000000 \\
0.000000 & 0.000000 & 0.000000 & 1.000000
\end{bmatrix} \tag{18}
$$

$$
{}^{0}T_{6,\mathrm{MAT}}\Big(\mathbf{q}^{(2)}\Big) = {}^{0}T_{6,\mathrm{RDK}}\Big(\mathbf{q}^{(2)}\Big) =
\begin{bmatrix}
-0.342346 & 0.288978 & 0.894031 & 2568.070293 \\
-0.873978 & 0.251354 & -0.415913 & -1453.601887 \\
-0.344908 & -0.923749 & 0.166510 & 1135.660391 \\
0.000000 & 0.000000 & 0.000000 & 1.000000
\end{bmatrix} \tag{19}
$$

$$
{}^{0}T_{6,\mathrm{MAT}}\Big(\mathbf{q}^{(3)}\Big) = {}^{0}T_{6,\mathrm{RDK}}\Big(\mathbf{q}^{(3)}\Big) =
\begin{bmatrix}
0.767463 & -0.640561 & -0.026114 & -1098.824930 \\
0.170714 & 0.243458 & -0.954769 & 1613.220607 \\
0.617945 & 0.728293 & 0.296198 & 1849.528656 \\
0.000000 & 0.000000 & 0.000000 & 1.000000
\end{bmatrix} \tag{20}
$$

IV. Analytical Inverse Kinematics

A. Kinematic Structure and Decoupling

A closed-form IK solution exists for the KR500 R2830 because it has a *spherical wrist* (the last three joint axes intersect). This permits position/orientation decoupling: first solve (q_1, q_2, q_3) from the wrist-center position, then solve (q_4, q_5, q_6) from a reduced wrist rotation.

Given a desired pose

$$
{}^{0}T_6 \triangleq \begin{bmatrix} R_{06} & p_{06} \\ \mathbf{0}^{\mathsf{T}} & 1 \end{bmatrix}, \tag{21}
$$

define the wrist center using the tool z-axis (third column of R_{06}) and the final offset $d_6 = 290$ mm:

$$
\hat{\mathbf{z}}_6 \triangleq R_{06} \begin{bmatrix} 0 \\ 0 \\ 1 \end{bmatrix}, \qquad p_{wc} \triangleq p_{06} - d_6\, \hat{\mathbf{z}}_6, \qquad d_6 = 290. \tag{22}
$$

Write $p_{wc} = [x_w \;\; y_w \;\; z_w]^{\mathsf{T}}$. The shoulder angle has two branches based on the in-plane radius

$$
\rho \triangleq \sqrt{x_w^2 + y_w^2}, \quad q_1^{(a)} = \operatorname{atan2}(-y_w, x_w), \quad q_1^{(b)} = q_1^{(a)} + \pi, \tag{23}
$$

where the π shift captures the flipped-shoulder configuration. For each shoulder branch, define

$$
B^{(a)} = +\rho, \qquad B^{(b)} = -\rho, \tag{24}
$$

and reduce (q_2, q_3) to a planar 2R problem via

$$
r \triangleq B - 500, \qquad z \triangleq 1045 - z_w. \tag{25}
$$

Combining the $(1025, 55)$ geometry into

$$
L \triangleq \sqrt{1025^2 + 55^2}, \quad \phi \triangleq \operatorname{atan2}(55, 1025), \quad A \triangleq 1300, \tag{26}
$$

the elbow solution follows from the law of cosines

$$
D \triangleq \frac{r^2 + z^2 - A^2 - L^2}{2AL}, \qquad |D| \le 1, \tag{27}
$$

with two elbow branches

$$
\gamma^{(\pm)} = \operatorname{atan2}\Big(\pm\sqrt{1 - D^2},\, D\Big), \tag{28}
$$

and

$$
q_2^{(\pm)} = \operatorname{atan2}(z, r) - \operatorname{atan2}\Big(L \sin\gamma^{(\pm)},\, A + L\cos\gamma^{(\pm)}\Big), \qquad q_3^{(\pm)} = \gamma^{(\pm)} - \phi. \tag{29}
$$

For each candidate (q_1, q_2, q_3), form

$$
R_{36} = R_{03}^{\mathsf{T}} R_{06}, \tag{30}
$$

with

$$
R_{03} = \begin{bmatrix} s_{23}c1 & c_{23}c1 & s1 \\ -s_{23}s1 & -c_{23}s1 & c1 \\ c_{23} & -s_{23} & 0 \end{bmatrix}, \tag{31}
$$

where $c1 = \cos q_1$, $s1 = \sin q_1$, $c_{23} = \cos(q_2 + q_3)$, and $s_{23} = \sin(q_2 + q_3)$. The wrist angles (q_4, q_5, q_6) are then extracted from R_{36} (Section B), with special handling near wrist singularities (Section C).

For the complete in-depth derivation of the analytical IK, please refer to the repository on GitHub: Click here for GitHub link.

B. Solution Branches

In the non-singular case, up to eight IK solutions exist due to branching in the shoulder, elbow, and wrist:

$$
(S, E, W) \in \{a, b\} \times \{+, -\} \times \{1, 2\}, \tag{32}
$$

yielding candidates $q^{(S,E,W)}$ of the form

$$
q^{(S,E,W)} \triangleq \begin{bmatrix} q_1^{(S)} & q_2^{(S,E)} & q_3^{(S,E)} \\ q_4^{(S,E,W)} & q_5^{(S,E,W)} & q_6^{(S,E,W)} \end{bmatrix}^{\mathsf{T}}. \tag{33}
$$

The (q_1, q_2, q_3) branches follow directly from (23)–(29). For each (S, E) pair, compute $R_{36}^{(S,E)}$ from (30) and extract wrist angles by first solving for the effective DH angles $(\theta_4, \theta_5, \theta_6)$ and then mapping to RoboDK joint variables.

Using the convention $\theta_4 = -q_4$, $\theta_5 = q_5$, $\theta_6 = \pi - q_6$, define

$$
c5 \triangleq R_{36}(2,3), \qquad s5 \triangleq \sqrt{R_{36}(2,1)^2 + R_{36}(2,2)^2}. \tag{34}
$$

If $s5 > \varepsilon$ (non-singular), the primary wrist branch is

$$
\theta_5^{(1)} = \operatorname{atan2}(s5, c5), \theta_4^{(1)} = \operatorname{atan2}(R_{36}(3,3), -R_{36}(1,3)), \qquad \theta_6^{(1)} = \operatorname{atan2}(-R_{36}(2,2), R_{36}(2,1)). \tag{35}
$$

and the flipped wrist branch is

$$
\theta_5^{(2)} = -\theta_5^{(1)}, \qquad \theta_4^{(2)} = \theta_4^{(1)} + \pi, \qquad \theta_6^{(2)} = \theta_6^{(1)} + \pi. \tag{36}
$$

Finally, map to RoboDK joints:

$$
q_4^{(W)} = -\theta_4^{(W)}, \qquad q_5^{(W)} = \theta_5^{(W)}, \qquad q_6^{(W)} = \pi - \theta_6^{(W)}. \tag{37}
$$

C. Singularities and Joint Limits

Reachability: The planar elbow solution requires (27) to satisfy $|D| \le 1$. If $|D| > 1$, the target wrist center is unreachable for that shoulder branch. In practice, D is clamped to $[-1, 1]$ prior to evaluating $\sqrt{1 - D^2}$ to avoid numerical issues from roundoff.

Wrist singularity ($s5 \le \varepsilon$): A wrist singularity occurs when

$$s5 = \sqrt{R_{36}(2,1)^2 + R_{36}(2,2)^2} \le \varepsilon, \tag{38}$$

corresponding to $\sin(\theta_5) \approx 0$ (i.e., $\theta_5 \approx 0$ or $\theta_5 \approx \pi$). In this case, θ_4 and θ_6 are coupled and the two wrist branches collapse into a single family. A consistent extraction can be performed by solving for the coupled angle and selecting (θ_4, θ_6) to best satisfy joint limits, then mapping to (q_4, q_5, q_6) using (37).

Joint limits and filtering: After generating candidates, solutions are wrapped to a consistent range and filtered by joint limits. For this model (degrees):

$$\begin{aligned} &q_1 \in [-185, 185], \quad q_2 \in [-130, 20], \quad q_3 \in [-100, 144], \\ &q_4 \in [-350, 350], \quad q_5 \in [-120, 120], \quad q_6 \in [-350, 350]. \end{aligned} \tag{39}$$

If multiple 2π-wrapped values satisfy limits, the solution closest to a reference configuration is selected to reduce discontinuities.

V. IK Verification

A. Round-Trip Procedure (FK → IK → FK)

The analytical IK was verified using a closed-loop consistency check. For each test joint configuration $\mathbf{q}_{\text{test}}$, a target pose was generated via forward kinematics,

$${}^{0}T_{6}^{\text{test}} \triangleq \text{FK}(\mathbf{q}_{\text{test}}), \tag{40}$$

then the analytical IK was applied to recover up to eight branch solutions,

$$\left\{\mathbf{q}^{(k)}\right\}_{k=1}^{N} \triangleq \text{IK}\left({}^{0}T_{6}^{\text{test}}\right), \qquad N \le 8, \tag{41}$$

and each candidate was pushed back through FK:

$${}^{0}T_{6}^{(k)} \triangleq \text{FK}\left(\mathbf{q}^{(k)}\right). \tag{42}$$

Pose agreement was quantified by a position residual and an orientation residual, same as (16) and (17) in the FK verification. A test was considered successful if at least one branch satisfied ${}^{0}T_{6}^{(k)} \approx {}^{0}T_{6}^{\text{test}}$ to numerical precision and the original configuration was recovered up to angle wrapping.

In addition, the same target poses ${}^{0}T_{6}^{\text{test}}$ were imported into RoboDK (base reference frame, flange tool frame) to cross-check that RoboDK reports consistent joint configurations. RoboDK may list more than eight "Other configurations" due to 360° wrap equivalents and wrist-singularity families; therefore, joint comparisons were performed in a wrap-aware sense, i.e.,

$$\Delta q_i^{(k)} \triangleq \text{wrap}_{180}\left(q_{\text{RDK},i} - q_i^{(k)}\right). \tag{43}$$

For each RoboDK solution, agreement is established if there exists a branch k such that $\max_i |\Delta q_i^{(k)}|$ is small and the FK re-check in (42) holds.

$${}^{0}T_{6}^{\text{test}} = \text{FK}(\mathbf{q}_{\text{test}}), \quad \{\mathbf{q}^{(k)}\} = \text{IK}({}^{0}T_{6}^{\text{test}}), \quad \text{FK}(\mathbf{q}^{(k)}) \approx {}^{0}T_{6}^{\text{test}}. \tag{44}$$

B. Representative Results

A total of 18 joint configurations were tested in MATLAB (including singular and non-singular wrist cases). For every test, all returned analytical branches satisfied the FK→IK→FK consistency check to numerical precision, and at least one branch recovered the original joint configuration up to angle wrapping and joint-limit conventions. Due to space constraints, three representative cases are summarized below.

TABLE III
Representative IK verification cases.

Case	$\mathbf{q}_{\text{test}}$ [deg]	N	Max error $(e_p,\ e_R)$
Home)	$[0, -90, 90, 0, 0, 0]$	3	(10^{-13}) mm, (10^{-6}) deg
Moderate	$[30, -20, 40, 10, -30, 60]$	4	(10^{-12}) mm, (10^{-6}) deg
Full-branch	$[0, -129, 20, 0, 10, 0]$	8	(10^{-12}) mm, (10^{-6}) deg

Cross-validation with RoboDK was performed by importing MATLAB-generated targets into a RoboDK station and inspecting RoboDK's *Other configurations* list. As expected, RoboDK frequently reports more solutions than the analytical $2 \times 2 \times 2$ branch structure due to angle-wrap equivalents (e.g., $\pm 180°$) and singular wrist families. Figures 3–4 show representative evidence for (i) the Home case (wrist singular behavior) and (ii) a "full-branch" target demonstrating many distinct configurations.

For the complete verification set (all test cases, branch outputs, and additional RoboDK screenshots), please refer to the GitHub repository.

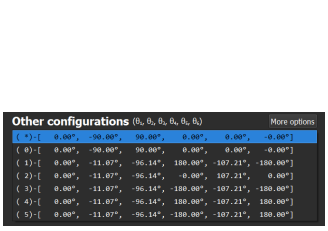

Home: RoboDK "Other configurations"

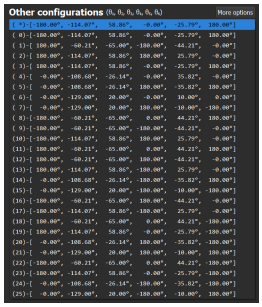

Full-branch: RoboDK "Other configurations"

Fig. 3. RoboDK reports multiple joint solutions for each target pose. Counts can exceed 8 due to wrap equivalents and singular families.

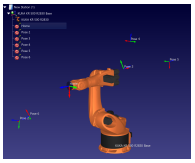

Station targets (Home and additional poses)

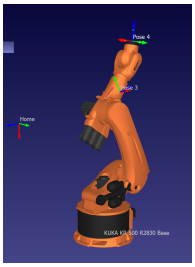

Full-branch pose

Fig. 4. Visual validation in RoboDK: multiple distinct joint configurations reach the same imported target pose when reference/tool frames are matched.

VI. Interactive Motion Planning Application

A. System Architecture

The interactive app connects waypoint input, FK/IK solvers, trajectory generation, and visualization in a single planning loop. The user provides a start and goal waypoint as either joint vectors $\mathbf{q} \in \mathbb{R}^6$ or Cartesian poses ${}^0T_6 \in SE(3)$. Cartesian waypoints are converted to joint space with the analytical IK solver and filtered by joint limits in (39). Motion is discretized over a fixed horizon T_f with N samples:

$$\tau_k = \frac{k}{N-1}, \qquad t_k = T_f\,\tau_k, \qquad k = 0, \ldots, N-1. \quad (45)$$

For each sample, the planner outputs a joint command $\mathbf{q}_k$, and the corresponding tool pose is evaluated by FK:

$${}^0T_{6,k} = \mathrm{FK}(\mathbf{q}_k). \quad (46)$$

When multiple IK branches exist, branch continuity is enforced by selecting the feasible solution closest to the previous sample:

$$\mathbf{q}_k = \arg\min_{\mathbf{q} \in \mathcal{S}_k} \left\| \mathrm{wrap}_\pi(\mathbf{q} - \mathbf{q}_{k-1}) \right\|_W, \quad (47)$$

where $\mathcal{S}_k = \{\mathbf{q} \in \mathrm{IK}({}^0T^d_{6,k}) \mid \mathbf{q}_{\min} \le \mathbf{q} \le \mathbf{q}_{\max}\}$. If $\mathcal{S}_k = \varnothing$, the app reports an infeasible segment and aborts execution.

B. MoveJ: Joint-Space Interpolation

MoveJ plans directly in joint space between $\mathbf{q}_0$ and $\mathbf{q}_f$. To avoid endpoint velocity discontinuities, a cubic time-scaling is used:

$$\sigma(\tau) = 3\tau^2 - 2\tau^3, \qquad \tau \in [0, 1]. \quad (48)$$

The commanded trajectory is

$$\mathbf{q}_k = \mathbf{q}_0 + \sigma(\tau_k)\,(\mathbf{q}_f - \mathbf{q}_0), \quad (49)$$

with velocity profile

$$\dot{\mathbf{q}}(t) = \frac{6\tau(1-\tau)}{T_f}\,(\mathbf{q}_f - \mathbf{q}_0), \qquad \tau = \frac{t}{T_f}. \quad (50)$$

This produces smooth joint motion and robust execution, while the end-effector path in Cartesian space is generally non-linear. The resulting poses are still available from (46) for animation and path inspection.

C. MoveL: Cartesian-Space Interpolation

MoveL enforces a linear tool-position path while maintaining continuous orientation interpolation. Let start and goal poses be ${}^0T_{6,0} = [R_0 \;\; p_0; 0 \;\; 1]$ and ${}^0T_{6,f} = [R_f \;\; p_f; 0 \;\; 1]$. Position is interpolated as

$$p_k = p_0 + \sigma(\tau_k)\,(p_f - p_0), \quad (51)$$

and orientation uses the matrix log/exponential map:

$$R_k = R_0 \exp\big(\sigma(\tau_k)\,\log\big(R_0^{\mathsf{T}} R_f\big)\big). \quad (52)$$

The desired pose sequence is

$${}^0T^d_{6,k} = \begin{bmatrix} R_k & p_k \\ \mathbf{0}^{\mathsf{T}} & 1 \end{bmatrix}, \quad (53)$$

and IK is solved at each k using the continuity rule in (47). This approach preserves Cartesian path intent while avoiding abrupt branch switching near singular regions.

D. GUI and Visualization

The GUI provides two waypoint panels (joint or Cartesian input), a mode selector (MoveJ/MoveL), and trajectory controls. After planning, the app displays time histories of all six joint angles and animates the robot in 3-D using the FK chain at each sample. Diagnostic messages are shown for unreachable Cartesian targets, joint-limit violations, and IK branch loss. In practice, this interface was used to compare MoveJ and MoveL behavior and verify that the generated motion remains feasible before export to simulation.

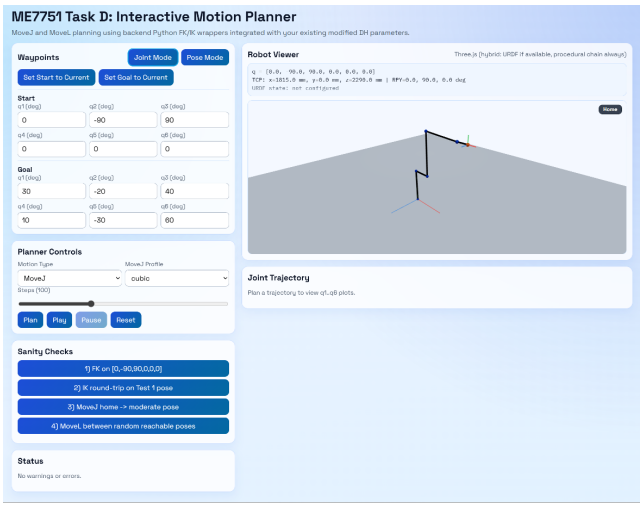

Fig. 5. Interactive motion-planning app outputs: waypoint controls, MoveJ/MoveL trajectory plots, and 3-D playback of the KR500 motion sequence.

VII. Conclusions

This project gave an in-depth understanding of deriving forward and inverse kinematics for an industry-relevant robot. Using a representitive KUKA robot for theme park applications, I was able to implement the FK/IK into a robust motion planning app. Future work includes building a scaled system with 3D printing and adding a mobile robot to the base to see the affect on the kinematics.